J Mater Sci: Mater Med (2010) 21:2087–2094
DOI 10.1007/s10856-010-4062-0

Effect of processing parameters on the microstructure and mechanical behavior of silica-calcium phosphate nanocomposite

Xueran Liu · Ahmed EI-Ghannam

Received: 18 December 2009 / Accepted: 15 March 2010 / Published online: 9 April 2010

Abstract Silica-calcium phosphate nanocomposite (SCPC) is a bioactive ceramic characterized by superior bone regenerative capacity and resorbability when compared to traditional bioactive ceramics. The aim of the present study is to evaluate the effect of processing parameters on the microstructure and mechanical properties of SCPC. Cylinders were prepared by pressing the ceramic powder at 200, 300 or 400 MPa and sintering at 900, 1000 or 1100°C for 3 h, respectively. XRD results indicate that the crystalline structure of the material is made of β-$NaCaPO_4$ and α-cristobalite solid solutions. The increase in sintering temperature results in an increase in the grain size and the formation of a melting phase that coats the grains. TEM analyses reveal that the melting phase is amorphous and rich in silicon. The mechanical properties of SCPC cylinders are dependent on the content of the melting phase and the microstructure of the material. The ranges of compressive strength and modulus of elasticity of the SCPC are 62–204 MPa and 6–14 GPa, respectively, which are comparable to those of cortical bone. The results suggest that the interaction between crystalline and amorphous phases modulated the mechanical behavior of SCPC. It is possible to engineer the mechanical properties of SCPC by controlling the processing parameters to synthesize various fixation devices for orthopedic and cranio-maxillofacial applications.

X. Liu
College of Material Science and Engineering, Jilin University, Changchun 130025, Jilin, People's Republic of China

X. Liu · A. EI-Ghannam (✉)
Department of Mechanical Engineering, University of North Carolina at Charlotte, Charlotte, NC 28223, USA
e-mail: arelgha@uncc.edu

1 Introduction

Ideally, the mechanical properties of orthopedic implants should be comparable to that of the host–bone at the implantation site in order to provide structural support and tissue guidance. In addition, the bioactivity of the implant material would allow for rapid integration with the bone, which enhances implant fixation and longevity. Hydroxyapatite (HA), tri-calcium phosphate (TCP), bioactive glass (BG), and calcium phosphate cement (CPC) are widely used as bone substitutes [1–6]. HA has a composition similar to that of mineral phase of bone and therefore bond to bone, however, its chemical stability limits its dissolution in physiological solutions. The limited solubility of HA inhibited the osteoconduction effect and resorbability of the material [7–9]. Moreover, the poor resorbability of HA implants limits the mechanical properties of bone at the implantation site. On the other hand, β-TCP is plagued by an unpredictable, fast rate of dissolution that may elicit adverse immunological response [10]. BG has an excellent surface reactivity, however, it has a dense nonporous structure that limits its resorbability in physiological solutions [11]. CPC has limitations due to its poor mechanical properties and slow in vivo biodegradation [12].

Silica-calcium phosphate nanocomposite (SCPC) is a bioactive ceramic characterized by superior bone regenerative capacity and resorbability when compared to HA and BG [13, 14]. Synthesis of SCPC with superior mechanical properties has been an important challenging goal. The compressive strength of cortical bone varies in the range of 100–230 MPa [15]. In a previous study, we prepared advanced dense SCPC with compressive strength in the range 55–285 MPa which is comparable to that of cortical bone [16]. The wide variations in the mechanical properties of polycrystalline SCPC are due to the variations in its

composition and microstructure. The effect of high sintering temperature and compact pressure on the grain size, phase composition and mechanical properties of SCPC has not been reported. In the present study, we prepare SCPC disks by powder metallurgy technique and use transmission electron microscopy to study the effect of processing parameters, pressure and temperature, on the grain size and phase transformation at the grain boundaries. The mechanical behavior of SCPC is correlated to the microstructure of the material.

2 Materials and methods

2.1 Materials preparation and processing parameters

SCPC (composed of 20.3 P_2O_5, 19.5 SiO_2, 40.7 CaO and 19.5 Na_2O in mol%) was prepared as previously reported [16, 17]. The original powders were calcined at 850°C for 2 h, ground, and sifted to a size range (250 nm–67 mm). To study the effect of processing parameters on the microstructure and mechanical properties, SCPC particles were uniaxially pressed into disks (10 mm dia. × 4 mm) at 200, 300 or 400 MPa using Instron 4400 R machine. The SCPC disks were sintered in air at 900, 1000 or 1100°C for 3 h at a heating rate of 2°C/min.

2.2 Structural characterization

2.2.1 X-ray diffraction analysis

The phase compositions of powdered samples of SCPC prepared under different compact pressures and sintering temperatures were determined by X-ray diffraction (XRD, X' Pert PRO) analysis with Ni-filtered Cu K (alpha) radiation at 45 kV and 40 mA.

2.2.1.1 Electron microscopy The morphology and elemental composition were characterized by scanning electron microscope–energy dispersive X-ray analysis (SEM–EDX). The samples were coated with gold and analyzed employing a JEOL JSM-6480 microscope with an accelerating voltage of 10 keV. The fine details of the interaction between SCPC grains after sintering at different compact pressures and sintering temperatures were analyzed using transmission electron microscope (TEM, Hitachi HF-2000 with an accelerating voltage of 200 kV) equipped with EDS system and energy dispersive X-ray analyzer (EDX, Oxford INCA EDS). The TEM samples were prepared by focused ion beam system (FIB, FEI Quanta 200 3D).

2.2.2 Density measurements

The relative density of the as-sintered SCPC was measured by the Archimedian method using deionized water as the medium. The porosity was obtained by calculating the relative density.

2.2.2.1 Mechanical testing Five replicates of each SCPC sample ($n = 5$) were compressed uniaxially to failure at a strain rate of 0.01% s^{-1}. On the stress–strain curve, the maximum stress value obtained from the curve was taken as the compressive strength of the SCPC sample and the modulus of elasticity of the SCPC sample was calculated by taking the slop of the linear portion of the stress–strain curve.

2.3 Statistical analysis

All the data were expressed as mean ± standard deviation (SD) and analysis of the results was carried out using Student's *t*-test. Statistical significance was considered at $P < 0.05$.

3 Results

3.1 XRD analysis of crystalline phase

XRD spectra of SCPC pressed at 200, 300 or 400 MPa and then sintered at 900°C for 3 h are shown in Fig. 1. Before

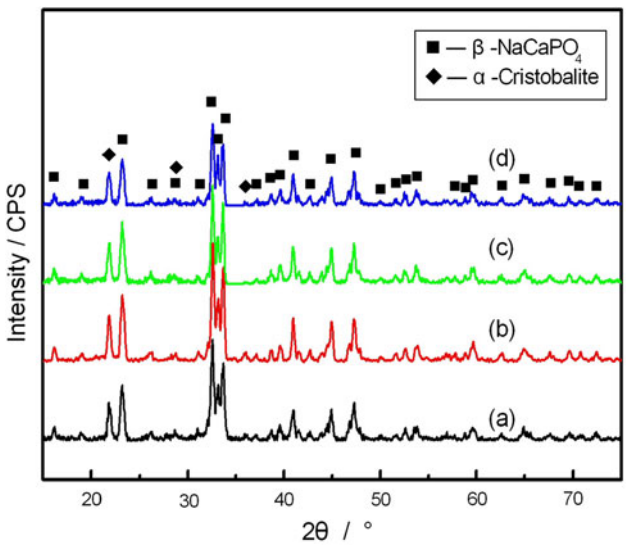

Fig. 1 XRD patterns of (*a*) SCPC pressed at 200 MPa before sintering, (*b*) pressed at 200 MPa and sintered at 900°C for 3 h, (*c*) 300 MPa/900°C/3 h, and (*d*) 400 MPa/900°C/3 h. SCPC prepared at the compact pressures had the same crystalline phases of β-$NaCaPO_4$ and α-cristobalite

sintering, SCPC material was composed of β-$NaCaPO_4$ and α-cristobalite (Fig. 1a). After sintering at 900°C, all samples had the same crystalline phases as SCPC before sintering (Fig. 1b–d). SCPC pressed at 200 MPa and sintered at 900, 1000 or 1100°C for 3 h had the main crystalline phases of β-$NaCaPO_4$ and α-cristobalite (Fig. 2). However, as the sintering temperature increased from 900 C to 1000 or 1100°C, a small tip indicating minor unknown phase appeared (Fig. 2b, c). It should be noted that with increasing the compact pressure and sintering temperature, the intensity of characteristic peaks of α-cristobalite decreased gradually. Table 1 shows the percent of the relative decrease of α-cristobalite phase after sintering compared with before sintering according to XRD data. As the compact pressure increased the percent of α-cristobalite phase decreased from 18.17 to 2.28. On the other hand, the increase in the sintering temperature result in a higher rate of decrease in the percentage of α-cristobalite for SCPC discs prepared at fixed pressure of 200 MPa.

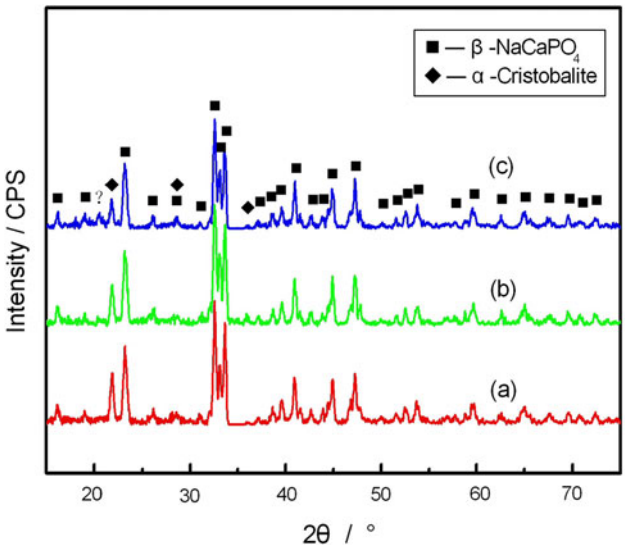

Fig. 2 XRD patterns of SCPC pressed at 200 MPa and sintered at: (*a*) 900°C, (*b*) 1000°C and (*c*) 1100°C for 3 h. The crystalline phases of the SCPC were mainly composed of β-$NaCaPO_4$ and α-cristobalite

Table 1 Effect of processing parameters on the percent of relative decrease of α-cristobalite phase compared with before sintering

	Pressure (MPa)			Temperature (°C)		
	200	300	400	900	1000	1100
(%) Decrease of α-cristobalite	2.28	8.77	18.17	2.28	21.39	45.33

SCPC samples were either pressed at various pressures then heated at fixed temperature (900°C) or pressed at a fixed pressure (200 MPa) and then treated at various temperatures

3.2 SEM–EDX analysis of SCPC Surface

The SEM morphology of SCPC pressed at 200, 300 or 400 MPa and sintered at 900°C for 3 h is shown in Fig. 3a, b and c, respectively. After sintering, the grain size of SCPC 200 MPa/900°C/3 h ranged from 0.3 to 1 μm (Fig. 3a). EDX analyses showed that the small round grains were silica crystals (black arrows) and the hexagonal grains were rich in sodium calcium phosphate (white arrows). The grain boundaries were found to be separated by a melting phase. The formation of the melting phase at the grain boundaries (Fig. 3a–c) correlated well with the decrease in the intensity of the XRD characteristic peaks of α-cristobalite (Fig. 1). Fig. 3a–c shows that the increase in compact pressure from 200 to 400 MPa resulted in a limited increase in the grain size and a significant increase from 2.28 to 18.17% in the percent of the melting phase (Table 1). Occasionally, nanosized pores in the size range of 30–200 nm were noticed at the grain boundaries and triple junctions.

Figure 4a and b show the morphology of SCPC pressed at 200 MPa and sintered at 1000 or 1100°C for 3 h. The grain size range of SCPC 200 MPa/1000°C/3 h increased from 0.3 to 2 μm (Fig. 4a) to (1–5 μm) after treatment at 1100°C/3 h (Fig. 4b). The particles of SCPC 200 MPa/1100°C/3 h appeared significantly coarse and were fully enveloped within the melting phase (Fig. 4b). The decrease in the percentage of α-cristobalite (Table 1) correlates well with the formation of the amorphous phase after thermal treatment at high temperature. Percent of the melting phase increased from 21.39% for SCPC 200 MPa/1000°C/3 h to 45.33% for 200 MPa/1100°C/3 h. Occasional cracks 0.5–4 μm long were observed at the interface between the melted phase and the SCPC grains (Fig. 4a, b).

Figure 5 demonstrates the EDX analyses of the different positions marked in Fig. 4a. EDX analyses revealed that the compositions of the hexagonal crystals (points A and B) were mainly O, Na, P, Ca and a minimal percentage of Si. Table 2 shows the atomic percentage of Na, Ca, P and Si on each position on the material surface. The composition of the melting phase (point C) was rich in Si, having minimal content of Na, P and Ca (Fig. 5c). The content of silicon for point C was 46.17 at.% indicating that the melting phase was Si-rich phase.

3.3 TEM–EDX analysis of SCPC microstructure

Figure 6 shows a TEM image of the microstructure of SCPC pressed at 200 MPa and sintered at 900°C for 3 h. The grain size ranged from 300 to 1000 nm and the melting phase separated the grain boundaries, which was consistent with the SEM observation (Fig. 3a). The selected area diffraction of region A (Fig. 6b) indicated that the melting

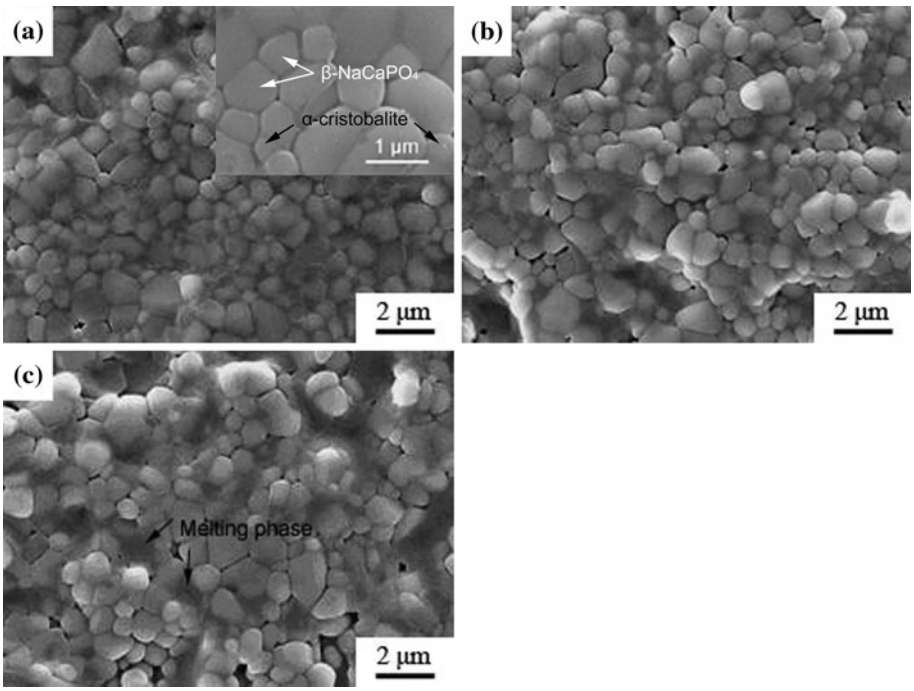

Fig. 3 SEM micrographies of SCPC pressed at different pressures and sintered at 900°C for 3 h: **a** 200 MPa, **b** 300 MPa and **c** 400 MPa. The grains were fused together during the sintering. The small round grains indicated a silica crystals (*black arrows*), and the hexagonal grains represented sodium calcium phosphate (*white arrows*)

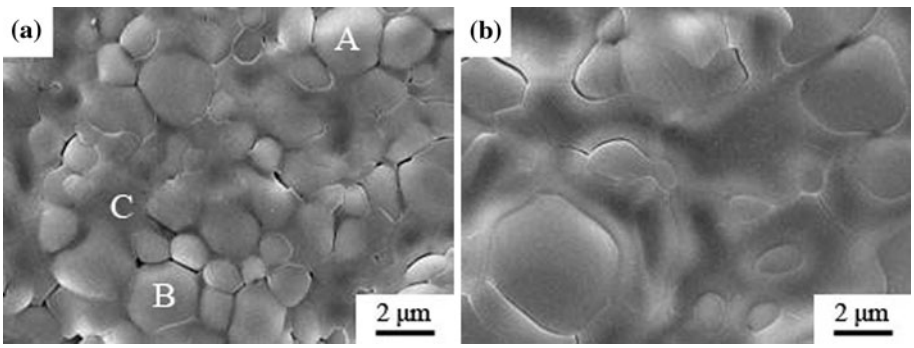

Fig. 4 SEM micrographs of SCPC pressed at 200 MPa and sintered at different temperatures for 3 h: **a** 1000°C and **b** 1100°C. The sintering temperature had a significant effect on the morphology of SCPC. The grains became coarse and the percent of the melting phase increased with increasing the sintering temperature

phase was amorphous. In addition, EDX analysis showed that the melting phase was silicon-rich (Fig. 6c). These results showed that crystalline silica transformed into the amorphous phase during sintering.

3.4 Measurement of the relative density of SCPC

Table 3 shows the effect of processing parameters on the relative density of SCPC. As the compact pressure and sintering temperature increased, the relative density of SCPC gradually decreased. With increasing the compact pressure from 200 to 400 MPa, the relative density decreased from 90.70 to 84.85%. Moreover, the relative density decreased from 81.32 to 78.92% with increasing the sintering temperature from 1000 to 1100°C. Thus the SCPC 200 MPa/900°C/3 h acquired the highest relative density of 90.70% and the microstructure was the most compact under all processing parameters.

3.5 Mechanical testing

Figure 7a and b show the compressive strength and modulus of elasticity of SCPC as a function of the compact pressure and sintering temperature. The compressive strength of SCPC decreased significantly with increasing the compact pressure (Fig. 7a). SCPC 200 MPa/900°C/3 h acquired a compressive strength of 205 ± 9 MPa, which was higher ($P < 0.001$) than that of SCPC 300 MPa/900°C/3 h (184 ± 9 MPa). Moreover, the compressive strength of the SCPC 300 MPa/900°C/3 h was significantly higher ($P < 0.004$) than that of SCPC 400 MPa/900°C/3 h (132 ± 6 MPa). As the sintering temperature increased, the compressive strength of SCPC decreased significantly and the malleability increased (Fig. 7b). SCPC 200 MPa/1000°C/3 h and 200 MPa/1100°C/3 h acquired mechanical strength of 119 ± 7 and 62 ± 12 MPa, respectively (Fig. 7b). The modulus of elasticity of SCPC significantly

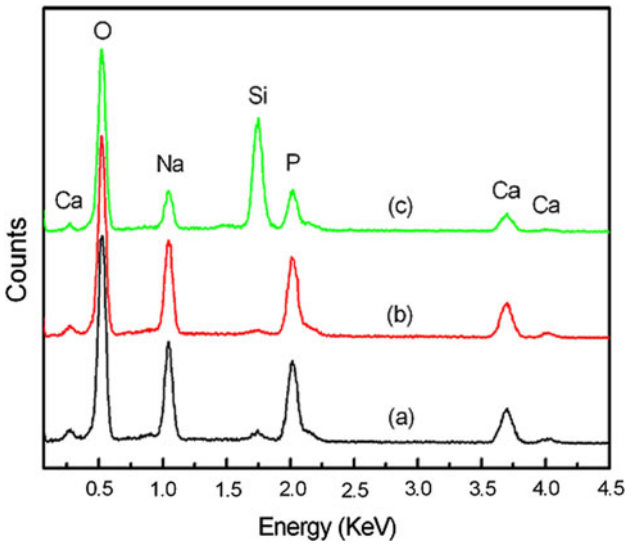

Fig. 5 EDX spectrums of selected points in Fig. 4a of SCPC 200 MPa/1000°C/3 h: (*a*) point A, (*b*) point B and (*c*) point C. The melting phase was α-cristobalite

Table 2 Compositions of different points for SCPC pressed at 200 MPa and sintered at 1000°C for 3 h corresponding to Fig. 4a (except oxygen element)

Mark	Element (at.%)			
	Na	P	Ca	Si
Point A	37	34	27	2
Point B	36	34	29	1
Point C	17	21	16	46

decreased with increasing the pressure and/or the temperature. The modulus of elasticity of SCPC was in the range of 6 ± 1 to 14 ± 1 GPa, which was comparable to the reported values for cortical bone [15].

4 Discussion

The processing parameters engineered the microstructure of SCPC and optimized its mechanical properties to be comparable to that of bone. The increase in the compact pressure or in the sintering temperature enhanced atomic diffusion at the grain boundaries, which resulted in an increase in the grain size and partial melting of the silica phase. The grains of the sodium calcium phosphate phase were coated with the amorphous silica-rich phase. In conjunction with the micro structural modifications, the compressive strength and modulus of elasticity of the material significantly decreased, however remained within comparable values to bone.

The increase in the powder compact pressure or the sintering temperature resulted in a significant increase in the grain size and the formation of a melting phase at the grain boundaries. As the sintering temperature increased from 900 to 1100°C, the grain size range increased from 0.3–1 to 2–5 μm and the percent of the melting phase significantly increased from 2.28 to 45.33% (Table 1). The increase in grain size of the silica phase is attributed to the diffusion of Na and Ca atoms from β-$NaCaPO_4$ to silica in addition to the phosphate-silicate ionic substitution. Previous studies in the literature [17] have showed that silicate-phosphate ionic substitution caused evident modifications of microstructure of SCPC. In conjunction with the increase in the percentage of melting phase in SCPC, XRD analyses (Figs. 1 and 2) revealed a decrease in the intensity of the characteristic peak of α-cristobalite suggesting that the melting phase is a silica-rich phase. Moreover, TEM–EDS analyses indicated that the melting phase is amorphous phase, which is mainly composed of silica structure incorporating Na, Ca and P elements. The transformation from α-cristobalite to β-cristobalite appeared at temperature of about 250°C [18]. Therefore, it is possible that the formation of the amorphous silica phase started during α to β partial transformation of cristobalite. These results suggest that the ionic diffusion at the interface between β-$NaCaPO_4$ and α or β-cristobalite resulted in a formation of a modified silicate structure that has a relatively low melting temperature. As the sintering temperature increased, more breakage of the Si–O bonds took place resulting in enhanced melting. Several studies reported that the crystallizing temperature of amorphous SiO_2 without any incorporated metal ions was over 1000°C [19, 20]. In the present study, SCPC pressed at different pressures and sintered at 900°C did not show any change in its crystalline structure of β-$NaCaPO_4$ and α-cristobalite. However, as the sintering temperature increased to 1000 or 1100°C, a small tip indicative of α-quartz appeared at 2-theta 20.521° in XRD patterns (Fig. 2b, c), which could be due to the crystallization of the amorphous phase. Data in the literature indicated that sample preparation using focused ion beam may affect the structure of the material and introduce surface damage [21–25]. However, encouraging results for alumina, magnesium aluminate spinel, and yttria-stabilized zirconia were reported [25]. Since the Si–O bond strength of ceramic is high, it is expected that the use of focused ion beam during sample preparation would have minimal effect of the structure modification of the SCPC material.

The thermal behavior of the SCPC phases during heat treatment played an important role in modifying the porosity of the material. SCPC phases had significantly different thermal expansion coefficient. It has been reported that, in the temperature range from 1000 to 1550°C, both β-$NaCaPO_4$ and α-cristobalite have positive thermal expansion coefficient, whereas β-cristobalite and the silica melt have negative thermal expansion coefficient [20, 26].

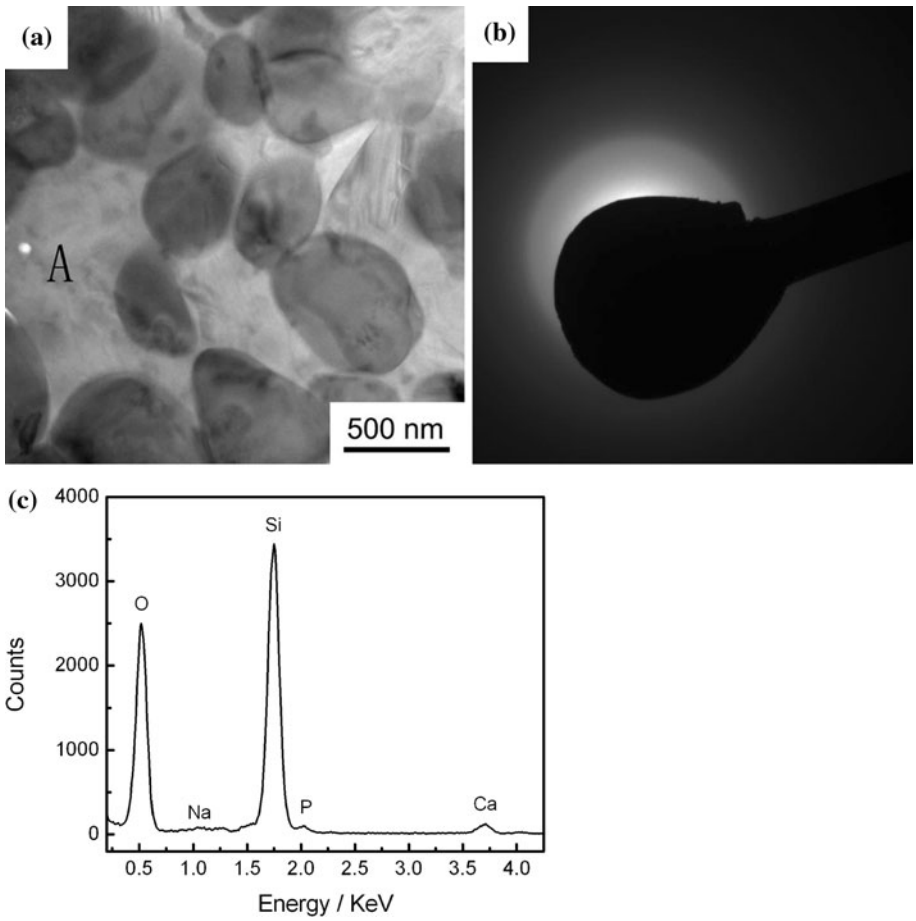

Fig. 6 **a** TEM micrograph of SCPC pressed at 200 MPa and sintered at 900°C for 3 h, **b** selected area diffraction pattern of the melting phase showed that it is non crystalline and **c** EDX spectrum of the non crystalline phase showing that it is Si-rich

Table 3 Effect of processing parameters on the relative density of SCPC

	Pressure (MPa)			Temperature (°C)		
	200	300	400	900	1000	1100
Relative density (%)	90.70	87.11	84.85	90.70	81.32	78.92

Therefore, the formation of nano pores and cracks in SCPC samples at 1000 or 1100°C is due to the difference in the thermal behavior of SCPC crystalline phases at high temperature. Moreover, the linear increase in the porosity of SCPC with increasing the compact pressure and sintering temperature (Table 3) correlates well with the increase in the percent of the melting phase in the material (Table 1).

In conjunction with the significant modification of the microstructure and porosity we observed significant changes in the mechanical properties of SCPC prepared under various pressures and temperatures. As the compact pressure and/or the sintering temperature increased, the mechanical properties decreased in the order 200 MPa/900°C/3 h > 300 MPa/900°C/3 h > 400 MPa/900°C/3 h > 200 MPa/1000°C/3 h > 200 MPa/1100°C/3 h. There were several factors affecting the mechanical properties of SCPC, such as porosity, grain size and the percent of the melting phase. The percent of the melting phase significantly increased with increasing the compact pressure, however, with minimal change in the grain size. Therefore, the decrease in the mechanical properties of the material is mainly due to the increase in the percent of the melting phase that led to separation of the grains. The reduction in the density of the grain boundaries in ceramic materials is known to facilitate crack propagation and reduce the mechanical strength. The development of cracks at the interface between the melting phase and the crystalline phases has contributed to the decrease in the mechanical strength (Fig. 4). Moreover, the decrease in the strength of the SCPC ceramic can also be attributed to the poor mechanical strength of the amorphous phase that lacks a crystalline configuration.

The compressive strength of cortical bone varies in the range of 100–230 MPa, and the modulus of elasticity ranges 7–30 GPa [15]. Although HA-coated implants are often used as load-bearing implants, the medical applications of pure HA ceramics are limited by its poor mechanical properties [27, 28]. Tricalcium phosphate (β-TCP) is widely used as bone substitute materials, however, the compressive and bending strength of sintered β-TCP are 83 and 21 MPa, respectively, which are lower

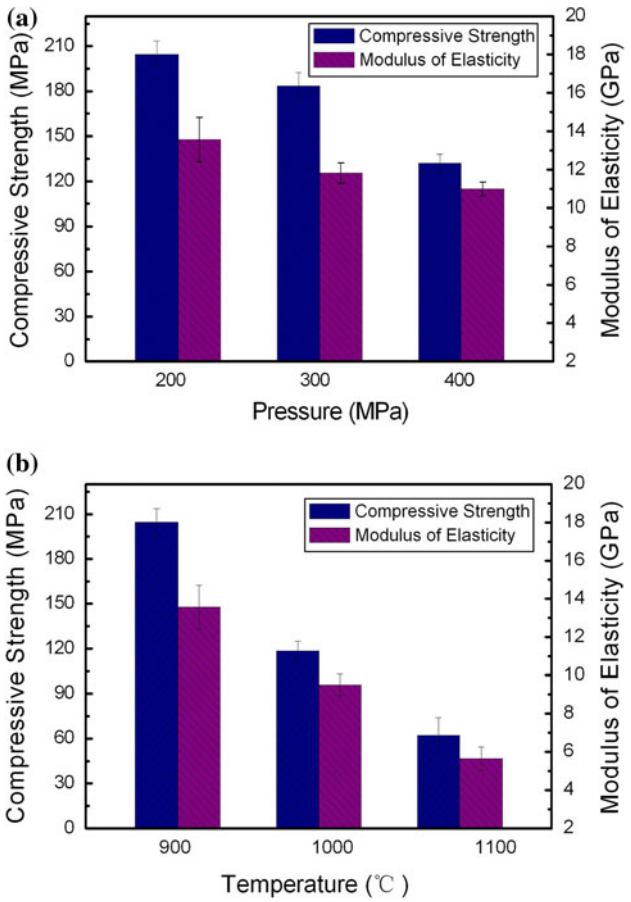

Fig. 7 Effects of **a** the pressure and **b** the temperature on the compressive strength and the modulus of elasticity of SCPC. Under all processing conditions, the strength and elasticity of SCPC were comparable to the corresponding values of bone. The compressive strength of cortical bone is 100–230 MPa and the modulus of elasticity is 7–30 GPa [15]

than those of the human bone [29, 30]. Doping dense β-TCP with MgO under vacuum increased the compressive strength to 301 MPa [31]. However, the nonporous compact structure of TCP or HA influenced the biocompatibility and degradability of the material [32–35]. SCPC has superior mechanical and biological properties when compared to HA and BG [14, 36]. Previous study has showed that the mechanical properties of SCPC was dependent on the Si content of the material and the compressive strength and modulus of elasticity of the same composition of dense SCPC50 were 54.66 MPa and 1.32 GPa, respectively [16]. These samples were prepared using porous ceramic particles in the size range 45–150 μm and were compacted manually at 360 MPa with zero holding time [16]. In the present study, the superior mechanical properties of SCPC50 cylinders are attributed to the use of nano size ceramic particles (250 nm–67 μm) and the employment of Instron machine for powder compaction which have produced highly dense cylinders. The present study further demonstrates that using higher pressure, temperature and longer thermal treatment duration allowed increasing the compressive strength and modulus of elasticity of SCPC to 118.48–204.57 MPa and 9.50–13.56 GPa, respectively, which are compatible to cortical bone. Under all processing parameters, only the mechanical properties of SCPC 200 MPa/1100°C/3 h fall below the target range. The superior mechanical properties of SCPC could be attributed to the high mechanical strength of the silica phase and to the fine grain microstructure. The presence of a high volume of grain boundaries in the crystalline structure of the material restricted the movement of dislocations and propagation of cracks during mechanical loading.

5 Conclusion

Compact pressure and sintering temperature significantly modified the SCPC microstructure and its mechanical properties. The increase in the sintering temperature or in the compact pressure enhanced atomic diffusion at the grain boundaries and hence facilitated crystal growth as well as partial melting of the silica phase. The sodium calcium phosphate crystals were coated with amorphous silica. In conjunction with the modification of the phase structure, the compressive strength, modulus of elasticity and brittleness of the material significantly decreased. However, under all processing conditions, the mechanical properties of SCPC were comparable to that of cortical bone. These results indicate that it is possible to engineer the mechanical properties for SCPC to be used as fixation devices for load-bearing applications in orthopedic and cranio-maxillofacial surgeries.

References

1. Alliot-Licht B, Delange GL, Gregoire M. Effects of hydroxyapatite particles on periodontal ligament fibroblast-like cell behavior. J Periodontol. 1997;68:158–65.
2. Den Hollander W, Patka P, Klein CP, Heidendal GA. Macroporous calcium phosphate ceramics for bone substitution: a trace study on biodegradation with 45Ca trace. Biomaterials. 1991;12:569–73.
3. Gan Y, Dai KR, Zhang P, Tang T, Zhu Z, Lu J. The clinical use of enriched bone marrow stem cells combined with porous beta-tricalcium phosphate in posterior spinal fusion. Biomaterials. 2008;29:3973–82.
4. Clavel-Sainz, Lopez-Prats F, Meseguer-Ortiz CL. In vitro behavior of adult mesenchyamal stem cells seeded on a bioactive glass ceramic in the SiO_2–CaO–P_2O_5 system. Acta Biomaterialia. 2008;4:1104–13.
5. Ohtsuki C, Kokubo T, Takatsuka K. Compositional dependence of bioactivity of glasses in the system CaO–SiO_2–P_2O_5: its in vitro evaluation. J Ceram Soc Jpn. 1991;99:1–6.

6. Sugawara A, Fujikawa K, Takagi S, Chow LC, Nishiyama M, Murai S. Histopathological and cell enzyme studies of calcium phosphate cements. Dent Mater J. 2004;23:613–20.
7. Costantino PD, Frendman CD. Synthetic bone graft substitutes. Otolaryngol Clin North Am. 1994;27:1037–74.
8. Suchanec W, Yoshimura M. Processing and properties of hydroxyapatite-based biomaterials for use as hard tissue replacement implants. J Mater Res. 1998;13:94–117.
9. Bagambisa FB, Joos U, Schilli W. Mechanisms and structure of the bond between bone and hydroxyapatite ceramics. J Biomed Mater Res. 1993;27:1047–55.
10. Eggli PS, Muller W, Schenk RK. Porous hydroxyapatite and tricalcium phosphate cylinders with two different pore size ranges implanted in the cancellous bone of rabbits. Clin Orthop. 1988;232:127–37.
11. Kim HM, Miyaji F, Kokubo T. Bioactivity of Na_2O–CaO–SiO_2 glasses. J Am Ceram Soc. 1995;78:2405–11.
12. Ambard AJ, Mueninghoff L. Calcium phosphate cement: review of mechanical and biological properties. J Prosthodont. 2006;15:321–8.
13. EI-Ghannam AR. Advanced bioceramic composite for bone tissue engineering design principles and structure–bioactivity relationship. J Biomed Mater Res. 2004;69A:490–501.
14. Gupta G, Kirakodu S, EI-Ghannam AR. Dissolution kinetics of a Si-rich nanocomposite and its effect on osteoblast gene expression. J Biomed Mater Res. 2007;80A:486–96.
15. Kokubo T, Kim HM, Kawashita M. Novel bioactive materials with different mechanical properties. Biomaterials. 2003;24:2161–75.
16. Gupta G, EI-Ghannam A, Kirakodu S, Khraisheh M, Zbib H. Enhancement of osteoblast gene expression by mechanically compatible porous Si-rich nanocomposite. J Biomed Mater Res. 2007;81B:387–96.
17. EI-Ghannam A, Ning CQ. Effect of bioactive ceramic dissolution on the mechanism of bone mineralization and guided tissue growth in vitro. J Biomed Mater Res. 2006;76A:386–97.
18. Altamirano-Juárez DC, Carrera-Figueiras C, Garnica-Romo MG, Mendoza-López ML, Ortuño-López MB, et al. Effects of metals on the structure of heat-treated sol–gel SiO_2 glasses. J Phys Chem Solids. 2001;62:1911–7.
19. de G, Tapfer L, Catalano M, Battaglin G, Caccavale F, Gonella F, et al. Formation of copper and silver nanometer dimension clusters in silica by the sol–gel process. Appl Phys Lett. 1996;68:3820–2.
20. Brückner R. Properties and structure of vitreous silica. J Non-Cryst Solids. 1970;5:123–75.
21. Ma L. Comparison of different sample preparation techniques in TEM observation of microstructure of INCONEL alloy 783 subjected to prolonged isothermal exposure. Micron. 2004;35:273–9.
22. Beia H, Shim S, Miller MK, Pharr GM, George EP. Effects of focused ion beam milling on the nanomechanical behavior of a molybdenum-alloy single crystal. Appl Phys Lett. 2007;91:111915.
23. Holzer L, Muench B, Wegmann M, Gasser P, Flatt RJ. FIB nanotomography of particulate systems-part I: particle shape and topology of interfaces. J Am Ceram Soc. 2006;89(8):2577–85.
24. Wilson JR, Kobsiriphat W, Mendoza R, Chen H-Y, Hiller JM, Miller DJ, et al. Three-dimensional reconstruction of a solid oxide fuel cell anode. Nat Mater. 2006;5(7):541–4.
25. Wu HZ, Roberts SG, Mobus G, Inkson BJ. Subsurface damage analysis by TEM and 3D FIB crack mapping in alumina and alumina/5 vol.% SiC nanocomposite. Acta Mater. 2003;51(1):149–63.
26. Yamahara K, Okazaki K, Kawamura K. Molecular dynamics study of the thermal behaviour of silica glass/melt and cristobalite. J Non-Cryst Solids. 2001;291:32–42.
27. de Groot K. Bioceramics consisting of calcium phosphate salts. Biomaterials. 1980;1:47–50.
28. Du C, Cui FZ, Zhu XD, de Groot K. Three-dimensional nano-HAP/collagen matrix loading osteogenic cells in organ culture. J Biomed Mater Res. 1999;44:407–15.
29. Bandyopadhyay A, Bernard S, Xue W, Bose S. Calcium phosphate based resorbable ceramics: influence of MgO, ZnO, SiO_2 dopants. J Am Ceram Soc. 2006;89:2675–88.
30. Kannan S, Lemos A, Rocha JHG, Ferreira JMF. Characterization and mechanical performance of the Mg-stabilized β-$Ca_3(PO_4)_2$ prepared from Mg-substituted Ca-deficient apatite. J Am Ceram Soc. 2006;89:2757–61.
31. Dantas ACS, Greil P, Müller FA. Effect of CO_3^{2-} incorporation on the mechanical properties of wet chemically synthesized β-tricalcium phosphate (TCP) ceramics. J Am Ceram Soc. 2008;91:1030–3.
32. Rodriguez-Lorenzo LM, Vallet-Regi M, Ferreira JMF. Fabrication of hydroxyapatite bodies by uniaxial pressing from a precipitated powder. Biomaterials. 2001;22:583–8.
33. Wiltfang J, Merten HA, Shlegel KA, Kloss FR, Rupprecht S, Lessler P. Degradation characterization of α and β tri-calcium-phosphate (TCP) in minipigs. J Biomed Mater Res. 2002;63:115–21.
34. Kalita SJ, Bhardwaj A, Bhatt HA. Nanocrystalline calcium phosphate ceramics in biomedical engineering. Mater Sci Eng C. 2007;27:441–9.
35. Lu J, Descaps M, Dejou J, Koubi G, Hardouin P, Lemaitre J, et al. The biodegradation mechanism of calcium phosphate biomaterials in bone. J Biomed Mater Res. 2002;63B:408–12.
36. EI-Ghannam A, Ning CQ, Mehta J. Cyclosilicate nanocomposite: a novel resorbable bioactive tissue engineering scaffold for BMP and bone-marrow cell delivery. J Biomed Mater Res. 2004;71A:377–90.